IEEE Access
Multidisciplinary | Rapid Review | Open Access Journal

Received March 31, 2019, accepted April 24, 2019, date of publication May 10, 2019, date of current version May 22, 2019.

Digital Object Identifier 10.1109/ACCESS.2019.2916077

Design and Fabrication of a Custom-Dielectric Fresnel Multi-Zone Plate Lens Antenna Using Additive Manufacturing Techniques

JAMES M. MONKEVICH, (Senior Member, IEEE), AND GREGORY PETER LE SAGE, (Member, IEEE)
United States Government, Washington, DC 20520, USA

Corresponding author: Gregory Peter Le Sage (lesagegp@gmail.com)

ABSTRACT Dielectric flat plate lens antennas fabricated using 3D printing offer several attractive designs features including volumetric efficient geometries, beam-steering capabilities, and relative ease of fabrication. This paper seeks to synthesize and optimize a lens design for microwave applications utilizing additive manufacturing techniques to implement custom-tailored dielectric materials that overcome the inadequacies of commercially available dielectric resources. Starting with a multi-dielectric Fresnel zone plate lens geometry previously reported in this paper, techniques are implemented to achieve customized dielectric properties. A study of 3D printing materials is conducted to identify commercially available supplies that offer appropriate dielectric properties. Measurement techniques are reviewed to verify the accuracy of the material characteristics (both dielectric constant and loss tangent). Finally, three inhomogeneous concentric-ring lens designs are manufactured using the proposed methods and evaluated to assess the overall performance of the antenna gain patterns and beam-steering capabilities. The result is a low-profile antenna configuration, offering simple, and low-cost fabrication, which can be integrated into compact microwave wireless system applications.

INDEX TERMS Additive manufacturing, aperture antennas, beam-steering, dielectric constant, directional antennas, flat lens antenna, Fresnel zone plate lens, microwave antenna.

I. INTRODUCTION/BACKGROUND

Lens Structures offer well-known canonical methods for transforming plane-wave radiation fields into spherical waves that converge on a singular focal point. These structures can achieve high-gain, directive beams and by simply translating the feed linearly about the focal point, allow one to implement beam scanning capabilities. Historically, lens structures have been created using subtractive manufacturing techniques–such as machining a lens profile on a single slab of dielectric material [1]. More recently, research has included mechanically perforating a dielectric material to achieve custom dielectric properties, which are then used to create flat graded-index (GRIN) lenses. One limitation to this technique is that the perforations are often required to be very closely spaced, which makes fabrication very difficult and time consuming, and thus expensive [2].

In this paper, additive manufacturing techniques (3D Printing) are investigated to implement a Fresnel zone plate lens (FZPL) design. FZPL geometries are compact, lightweight, and can be used in close proximity to the associated feed antenna, making this type of antenna desirable for wireless systems applications. While the FZPL design has been reported previously in literature; the goal in this work is to extend the analysis and implementation of a multi-zone lens and to assess the material losses, realized gain, and efficiency performance of the structure. The focus is on achieving a realized gain of 30dBi, requiring precise control of the dielectric constant (including the loss tangent). Previous work presented the FZPL concept, but provided normalized gain results and did not thoroughly evaluate dielectric performance. Generalized equations are provided for a planar multi-dielectric lens along with a discussion of our design trade-offs. Simulations are conducted in ANSYS HFSS software to verify and optimize the performance of the lens structure.

Methods are developed to accurately manufacture custom-dielectric materials by including periodic air gaps. Two commonly used 3D printing techniques are stereo-lithography apparatus (SLA) and fused-deposition modeling (FDM).

The associate editor coordinating the review of this manuscript and approving it for publication was Shafi Shahsavar Mirza.

Both techniques are utilized to create custom-dielectric structures. They are then measured using a waveguide resonant cavity that provides both dielectric constant and loss tangent at several frequencies. Additionally, a 3D printed material characterization method specifically suited to FDM printing is presented that significantly reduces the cost of the dielectric measurement.

Finally, three lens designs are fabricated utilizing both SLA and FDM custom-dielectric materials. Antenna pattern measurements are presented, confirming the performance of the overall antenna system, along with a comparison to HFSS simulations. Included in the measured results is a study in which the feed horn is offset from the focal point of the lens to demonstrate the beam-steering capability of the structure.

II. LENS LAYOUT/DESIGN

A variety of flat-plate lens designs have been previously reported in literature including: graded index lenses [3], [4] and FZPLs [5], [6]. The key tradeoff between these two structures is that FZPLs can be built with a thinner configuration than GRIN lenses. This is analogous to a phased array that is built with relative phased weights (in the FZPL case, where it corrects phase zonally) and a true-time weighted array (in the GRIN design, where it compensates phase across the whole structure). Hence operating bandwidth is compromised to allow for a thinner structure.

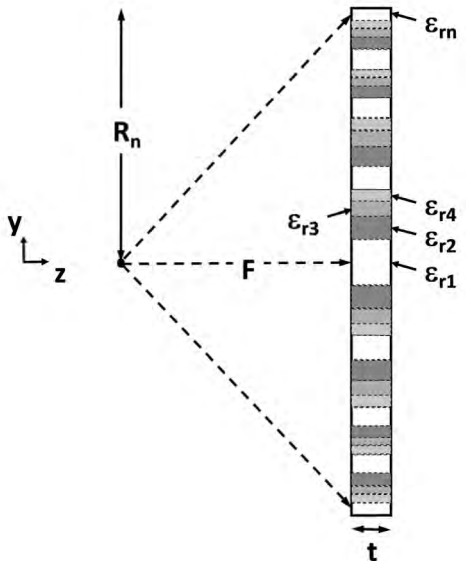

FIGURE 1. FZPL geometry, dielectric configuration, and plane-wave focusing effect.

Fig. 1 details the FZPL layout, dielectric configuration, and focusing effect for a plane-wave illumination.

The below equations, (1) and (2), provide the formulas to calculate the outer radius and the dielectric properties for each full-wave zonal and sub-zonal ring [5]. The key constraint is that the dielectric constant can vary between air ($\varepsilon_r = 1$) and commercially available plastic/resin materials that can be reasonably (and repeatedly) 3D printed. This constraint significantly limits the materials that can be selected for the lens since the bulk dielectric constant needs to be relatively high, and the material losses should be as low as possible. This topic is re-visited in the next section regarding customization of dielectric materials.

$$R_n = \sqrt{\left(\frac{2n\lambda F}{S}\right) + \left(\frac{n\lambda}{S}\right)^2} \tag{1}$$

$$\varepsilon_{rn} = \varepsilon_{r1}\left[1 + \left(\frac{1}{t}\right)\left(1 - \frac{n-1}{S}\right)\right]^2 \tag{2}$$

In the equations above, R_n is the outer radius and ε_{rn} is the dielectric constant for each ring. Additionally, Z is the number of zones, S is the number of sub-zones, F is the focal length, t is the thickness in wavelengths, and $n = 1, 2, \ldots S^*Z$.

Two lens geometries were designed for 20GHz with a selected F/D of 0.375, which matches a readily available wide-band (18 to 26.5GHz) feed antenna. The goal for this study was to achieve a lens structure with high-gain (~27-33dBi), which required an accurate understanding of material properties–including the dielectric losses. The frequency range and overall size of the lens were based on maximum printable volumes of several commercial SLA 3D printers. The first lens design represented what could be achieved in a single print volume, while the second design was sized to be printed in quarters (resulting in a 2X lens). Three total lenses were fabricated: a 1X SLA, a 2X SLA, and a 1X hybrid-FDM.

TABLE 1. 20GHz design; Z = 3, S = 4; thickness = 14.990mm; NanoTool material.

Inner Radius, mm	Outer Radius, mm	Effective ε_r
0.000	22.802	1.000
22.802	32.680	3.063
32.680	40.548	2.250
40.548	47.416	1.563
47.416	53.671	1.000
53.671	59.506	3.063
59.506	65.034	2.250
65.034	70.328	1.563
70.328	75.436	1.000
75.436	80.395	3.063
80.395	85.230	2.250
85.230	89.962	1.563

Tables 1 and 2 provide the radius of each sub-zonal ring, along with the required dielectric constants. Initially HFSS was used to assess the veracity of the designs, as shown in Fig. 2. The models were created by using the calculated dielectric constants as bulk material properties. The initial model assumed that the appropriate dielectric constants could be created and focused on the overall design. The simulated results for the two designs predicted 26.8dBi and 33.5dBi gain would be obtained. An open-ended waveguide feed was used in the simulations that provided a different pattern than our selected feed. The focal length was not re-optimized versus frequency for the plots in Fig. 2.

TABLE 2. 20GHz design; Z = 6, S = 4; thickness = 14.990mm; NanoTool material.

Inner Radius, mm	Outer Radius, mm	Effective ε_r
0.000	32.029	1.000
32.029	45.605	3.063
45.605	56.230	2.250
56.230	65.360	1.563
65.360	73.554	1.000
73.554	81.095	3.063
81.095	88.152	2.250
88.152	94.833	1.563
94.833	101.212	1.000
101.212	107.343	3.063
107.343	113.266	2.250
113.266	119.012	1.563
119.012	124.607	1.000
124.607	130.069	3.063
130.069	135.414	2.250
135.414	140.656	1.563
140.656	145.806	1.000
145.806	150.873	3.063
150.873	155.865	2.250
155.865	160.790	1.563
160.790	165.654	1.000
165.654	170.461	3.063
170.461	175.216	2.250
175.216	179.923	1.563

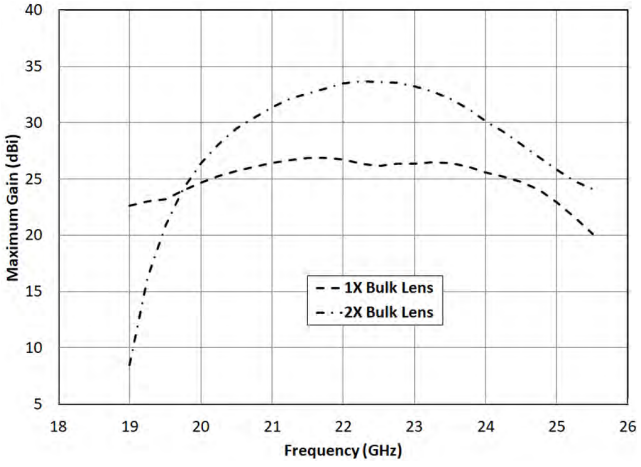

FIGURE 2. HFSS bulk modeling swept gain results.

III. CUSTOMIZATION OF DIELECTRIC MATERIALS

It is not possible to purchase dielectric materials with the exact specifications shown in Tables 1 and 2. Instead, the authors investigated a path similar to techniques proposed in [2] through [6], where the dielectric constant of a bulk material is adjusted by varying the fill factor (or infill percentage) of the object. In the paper by Imbert *et al.* [2] this was accomplished by using subtractive techniques (CNC machine) to drill holes in a solid piece of Rogers TMM6 dielectric. This technique is somewhat limiting because of the spacing required between holes–which can easily lead to fractures in the bulk material. Additionally, the holes required are similar in size to CNC cutting tools, which limits the overall hole shape. In this paper, the authors investigated additive manufacturing processes similar to those in [3] and [6] to implement the design. In this case, both dielectric constant and loss tangent are evaluated to ensure that an efficient structure is realized.

For the lenses reported in this paper, the authors utilized both SLA and FDM printing. Fig. 3 provides an illustration of the geometry for the SLA printed dielectric material.

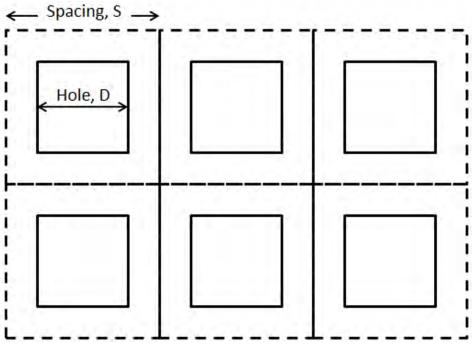

FIGURE 3. Hole configuration to obtain custom dielectric properties.

By adjusting the hole dimension (D) and the spacing (S), the bulk dielectric constant can be varied between that of the bulk material (ε_{bulk}) and that of air (ε_0). Square holes were chosen because the minimum solid thickness between perforations is greater compared to the minimum solid thickness available between round holes. Since additive manufacturing is limited by minimum feature thickness, square holes allow more numerous, closely spaced perforations. The below equations describe the relationship between dielectric material properties, fill factor, hole geometry, and surface area. It is interesting to note that equation (6) is the Wiener maximum bound defined in effective medium theory [7]. Intuitively this makes sense since the infill inclusions that are added are not randomly oriented, hence the depolarization factor would be zero.

$$Fill\ factor = ff = \frac{SA_{plastic} - SA_{hole}}{SA_{plastic}} = \frac{S^2 - D^2}{S^2} \quad (3)$$

$$ff = \frac{\varepsilon_{r,custom} - \varepsilon_{r,hole}}{\varepsilon_{r,bulk} - \varepsilon_{r,hole}} \quad (4)$$

$$D = S\sqrt{(1 - ff)} \quad (5)$$

$$\varepsilon_{custom} = ff^* \varepsilon_{bulk} + (1 - ff)^* \varepsilon_{hole} = \varepsilon' - j\varepsilon'' \quad (6)$$

$$\tan\delta_{custom} = ff * tan\delta_{bulk}\left(\frac{\varepsilon_{r,bulk}}{\varepsilon_{r,custom}}\right) + (1 - ff)\tan\delta_{hole}\left(\frac{\varepsilon_{r,hole}}{\varepsilon_{r,custom}}\right) \quad (7)$$

Of note, the loss tangent of the printed dielectric improves with the addition of holes since air is lossless. This is useful because it helps to control losses within the structure that would otherwise reduce performance of the FZPL. This fact favors a bulk dielectric constant that is high even if loss tangent is marginally higher, since more perforations will be used and the loss tangent of air is essentially zero.

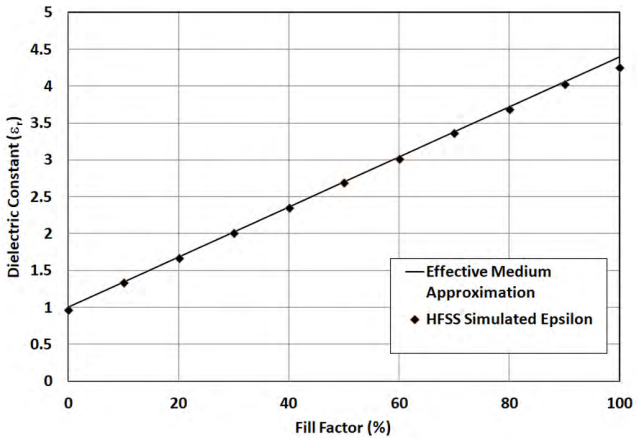

FIGURE 4. Comparison of resonant cavity simulation and effective medium approximation (2-inch diameter cavity filled with PREMIX TP20280 with 1-mm unit cells to implement various fill factors using square holes).

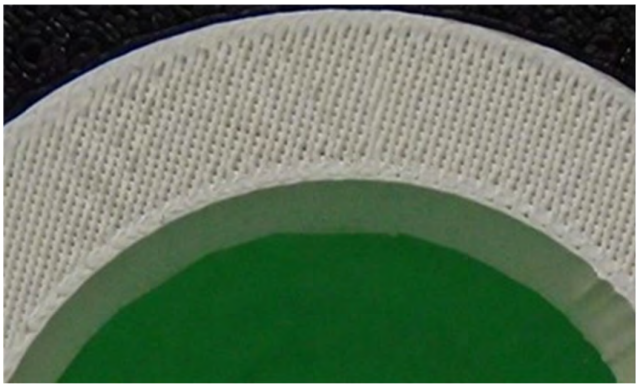

FIGURE 5. Linear infill pattern used to vary infill percentage.

Fig. 4 compares the effective medium approximation of dielectric constant computed using (6) to an HFSS simulation of a filled resonant cavity with various fill factors. These simulations are identical to the experimental measurements presented in section IV and the result confirms that equation (6) is accurate.

Printing with SLA offers the best spatial resolution, where commercial vendors can routinely achieve feature sizes of 50-micrometers. Extrusion with FDM is typically limited to an X-Y resolution of 300-400 micrometers, determined by the size of the print nozzle [8] and [9]. Utilizing the design where epsilon is determined by 3D printing small holes, SLA printing offers an advantage due to the superior resolution. For the lens manufactured using FDM, the highest dielectric constant rings required hole-dimensions below the print resolution. In this case it was necessary to adjust the infill percentage to introduce air into the internal structure. This corresponds to a small displacement of the FDM print head at each pass when depositing the plastic to create an offset linear infill pattern (see Fig. 5). The infill can be implemented as rows of alternating plastic and air, hexagonal holes, or other more complex configurations depending on the 3D printer used [10]. For this paper, the linear infill pattern proved to be sufficient. The authors did find it necessary to compute the infill percentage using measured material weights since 3D printing capabilities introduce inaccuracies into the process. Some printers (including the Fortus printer used in this study) only support discrete infill percentages (typically 10%, 25%, 50%, and 100%), while others require calibration to hit a specific infill percentage. Equation (8) provides details for the computation.

$$ff = \frac{Sample\ Weight}{Solid\ Weight} = \frac{Sample\ Weight}{Print\ Volume \times Specific\ Gravity} \tag{8}$$

Prior to the printing process, various print materials were investigated [11] to identify those with appropriate properties (both dielectric constant value and loss tangent). The key identified trade-offs were material losses (where SLA is roughly an order of magnitude worse than FDM), print resolution (where SLA outperforms FDM), and mechanical complexity (where SLA requires model features which allow uncured SLA resin to drain). The next section provides details of the measurement techniques used to characterize the test samples.

IV. DIELECTRIC MEASUREMENT TECHNIQUES

There are many ways to characterize the dielectric constant of a material, including: free space transmission, cavity perturbation, insertion of samples into waveguide sections, capacitive measurement, and filled resonant cavity measurement [12] through [15]. In all cases, the changes of RF properties, with and without the presence of the dielectric, allow characterization of the material.

Use of a resonant cavity limits the measurement to individual frequencies, but this technique is also most accurate among dielectric measurement methods. Additionally, the resonant cavity method can be performed without calibration of the network analyzer since the technique only requires relative amplitude values to collect the resonance data. In the microwave range, dielectric properties of the materials do not vary significantly with frequency. The results collected at the resonant frequencies of the cavities used for this experiment are valid at our operating frequency. Multiple resonant modes were measured to obtain the results presented here. Consequently, a range of frequencies are possible for each measurement; and multiple frequency measurements allow collection of statistics for more accurate results.

Measurement of changes of resonant peaks of S_{21}, with and without dielectric material filling a resonant cavity, determined dielectric constant. Measurement of changes of half-power bandwidths (Q) revealed loss tangent. Since all samples are 3D printed, the authors generated dielectric samples that completely filled the resonant test cavities.

Measurements related to this project use cylindrical cavities with two coaxial coupling probes on the cavity axis. The probes are flush with the cavity wall, meaning that the center pin did not protrude in to the cavity. Thus, the cavity is highly under-coupled. The Q circle for any resonance is a small circle at the periphery of the Smith chart. This is

important since introduction of dielectric fill could otherwise influence not only cavity resonance but the coupling coefficient. Cavity coupling needs to measure, but not affect the resonant property of the cavity.

Based on the cylindrical cavity geometry, examination of the field structure [16] and [17] shows that the visible modes will be TM_{0n0}. The probes couple to E_z on axis (r = 0). Only these modes were evident on the network analyzer despite the fact that in order of frequency, other modes resonate. The coupling configuration was optimized to excite only TM_{0n0} modes and provided peaks in S_{21}.

The formula for the resonant frequency of TM_{0n0} modes in a cylindrical cavity is as follows [16]:

$$(f_r)\, TM^z_{0n0} = \frac{c}{2\pi\sqrt{\varepsilon_r}}\left(\frac{\chi_{0n}}{a}\right) \tag{9}$$

where 'a' is the cavity radius and X_{0n} are the zeros of the $J_0(x)$ Bessel function. For a dielectric filled cavity, resonant frequency scales as the inverse of the square root of the relative dielectric constant.

For the empty cavities, resonances were well above the noise floor for TM_{010}, TM_{020}, TM_{030}, TM_{040}, TM_{050}, and TM_{060}. A spreadsheet was used to predict the same resonant frequencies shifted for an expected dielectric constant. After measurement of each resonant frequency, a best fit epsilon can be calculated by minimizing the sum of the squares of the differences between measured frequencies and expected frequencies for a selected dielectric constant. The best value for the dielectric constant minimizes the sum of the squares.

Loss tangent is determined by measuring the loaded (with dielectric sample) and unloaded (empty) quality factor 'Q' of the cavity [17]. Measuring several modes allows averaging of results for peaks that can be easily measured manually, with no curve fitting required.

Our FDM printed microwave lens was a hybrid of ABS filament used in a commercial 3D Printer (Stratasys Fortus 250 me), and PREMIX filament printed with a commercial hobbyist 3D printer (Flashforge). The Fortus printer does not allow adjustable fill factor, which is why the Flashforge printer was used. The PREMIX filament was tested with various fill factors. Prior to identifying PREMIX material, the authors attempted to create a custom filament by loading ABS with barium titanate using processes similar to [18] and [19]. The filament proved to be lumpy and very difficult to feed through an extruder for 3D printing. A custom 3D printer was built by one of the authors enabling a high extruder and bed temperature with a strong direct-feed filament stepper motor. However it was ultimately more effective to simply use the commercial solution from PREMIX. The resonant cavity measurement of Stratasys Black ABS and PREMIX resulted in good fits to expected linear and parabolic curves (see Figs. 6 and 7). The ABS curve is parabolic since it is plotted versus hole dimension.

Note that for the FDM materials, only linear infill achieved the required value of ε_r (3.06). Comparing sample weight

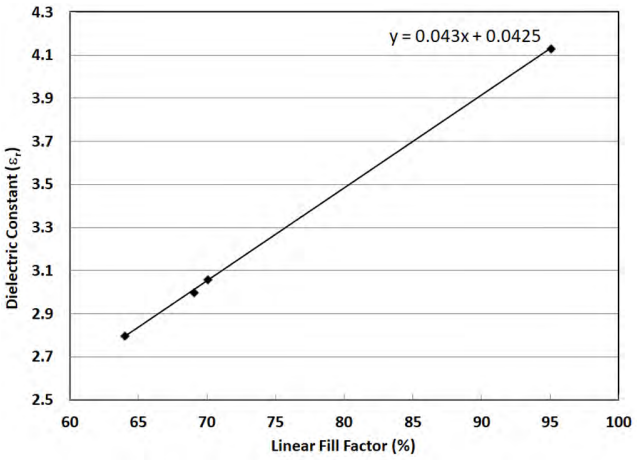

FIGURE 6. Resonant cavity measurement of PREMIX TP20280 ($\varepsilon_r = 3.063$) showing effect of fill factor on dielectric constant.

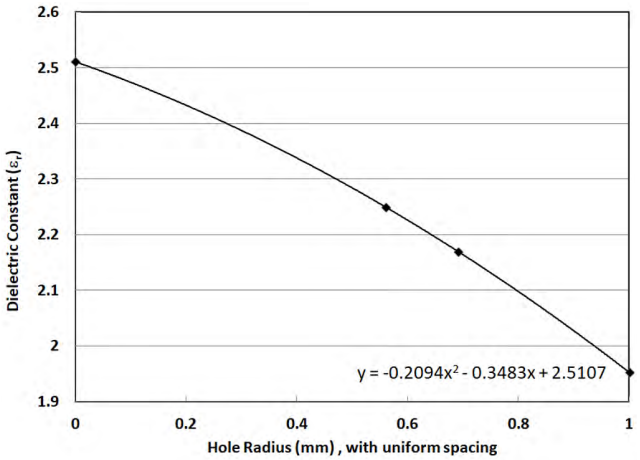

FIGURE 7. Resonant cavity measurement of Stratasys black ABS ($\varepsilon_r = 2.250$) for various hole dimensions.

to dielectric constant showed a linear relationship. Sample weight should always give an accurate measure of plastic versus air percentages for a uniform density 3D print, and thus an accurate prediction of the dielectric constant no matter the fill configuration.

A. CHARACTERIZING BULK PROPERTIES OF FDM FILAMENT

In the case of SLA, a solid printed sample gives bulk properties. With FDM 3D printing, a print with 100% infill will be nearly solid, but will not have the same properties as the bulk material–the plastic filament used to feed the printer. This is due to the fact that the FDM print process introduces a small amount of air into the solid printed sample since the plastic is extruded through a round nozzle.

For FDM prints, accurate designs require knowledge of the bulk (filament) material properties, which can be achieved using cavity perturbation measurement. A TE_{101} cavity was designed based on WR-90 waveguide with a length of 30-mm. The cavity was designed with a single flange using SolidWorks and then 3D printed and copper plated.

A coupling aperture was first simulated, then optimized empirically to achieve critical coupling for the empty cavity (resulting in an aperture diameter of 4.25-mm with an aperture thickness of 2-mm). The cavity also had 1.75-mm round holes at the center of the cavity broad wall, matching the diameter of the 3D printing FDM filament. The holes were located at a wall current minimum, to minimally affect cavity resonance. The holes allowed FDM filament to be inserted in to the center (E-field maximum) of the TE_{101} cavity. The filament fills 0.35% of the resonant cavity. Cavity perturbation formulas [20] allow determination of dielectric constant and loss tangent by noting the shift in resonant frequency and change in Q. For the cavity perturbation technique, dips in S_{11} measurement data are analyzed instead of resonant peaks in S_{21} data (which was used for the cavity resonance method).

The cavity perturbation measurement device was used to confirm both commercially specified dielectric constant and loss tangent values and to verify that the bulk filament had a slightly higher dielectric constant than a ''solid'' test sample printed with 100% infill. The results of the measurement are as follow in Table 3.

TABLE 3. Measured dielectric values of 3D printing materials.

ABS filament (Black) for Stratasys Fortus 250 me			
	Cavity Perturbation	Cavity Resonance of solid (100% infill) Puck	Published Value
ε_r	2.61	2.51	2.3-2.85
tanδ	0.0036	0.0042	0.0046-0.0053
PREMIX TP20280			
	Cavity Perturbation	Cavity Resonance of solid (100% infill) Puck	Published Value
ε_r	4.79	4.34	4.4
tanδ	0.0039	0.005	0.004

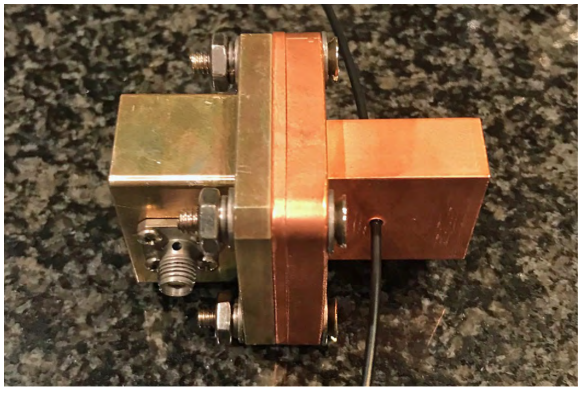

FIGURE 8. TE_{101} cavity device.

The cavity and coupling aperture used for this work is shown in Fig. 8 and has been posted to Thingiverse (object #2414931) [21]. The device was 3D printed with SLA and copper plated for roughly $300 total. Commercially available dielectric characterization kits including resonant cavity hardware and automated capture software costs in the range of $12-15K. Other cavity sizes can be created to cover other frequency ranges of interest. Lossy materials eventually preclude the filled cavity measurement because S_{21} becomes too small to measure peaks and half power widths accurately. Cavity perturbation allows accurate collection of data even for very lossy material.

Tables 4 and 5 below summarize the results of our tests. The SLA material selected was SOMOS NanoTool since it provided good performance, and was available at commercial 3D printing vendors. Table 4 lists the measured bulk properties of the 3D printing materials (prior to customization), while Table 5 provides the tailored results to obtain the dielectric values required for the lens.

TABLE 4. Measured dielectric values of bulk 3D printing materials.

Manufacturer / Material	Dielectric Constant	Loss Tangent
SOMOS 18120 (SLA)	3.160	0.033
SOMOS NanoTool (SLA)	3.356	0.015
PREMIX TP20280 (FDM)	4.79	0.0039
STRATASYS ABS (FDM)	2.61	0.0036

TABLE 5. Calculated vs. measured dielectric values of customized 3D printing materials.

Goal ε_r = 3.063, tan δ = 0.015; 0.525mm holes, 1.5mm space	
ε_r (difference)	tan δ (difference)
3.050 (0.013)	0.015 (0)
Goal ε_r = 2.250, tan δ = 0.008; 1.026mm holes, 1.5mm space	
ε_r (difference)	tan δ (difference)
2.320 (0.070)	0.012 (0.004)
Goal ε_r = 1.563, tan δ = 0.005; 2.616mm holes, 3mm space	
ε_r (difference)	tan δ (difference)
1.569 (0.006)	0.011 (0.006)
PREMIX TP20280	
Goal ε_r = 3.063, tan δ = 0.003; Linear Fill 70%	
ε_r (difference)	tan δ (difference)
3.052 (0.011)	0.005 (0.002)
STRATASYS ABS	
Goal ε_r = 2.250, tan δ = 0.004; 0.560mm holes, 3mm space	
ε_r (difference)	tan δ (difference)
2.244 (0.006)	0.006 (0.002)
Goal ε_r = 1.563, tan δ = 0.003; 1.453mm holes, 3mm space	
ε_r (difference)	tan δ (difference)
1.551 (0.012)	0.005 (0.002)

The overall FDM lens was a hybrid of ABS (generated using the Fortus commercial printer) to form the large structure and mechanical support, and PREMIX filament for the highest ε_r parts that were then snapped into place. The PREMIX TP20280 components of the microwave lens were made in four separate, identical sets of pieces since the print bed of the Flashforge 3D printer was not large enough to print the lens in one piece (see Fig. 9).

Based on the measured results, the authors constructed models of the lenses using SolidWorks with the design details listed in Table 5. Sections that contained air ($\varepsilon_r = 1$) were implemented as minimal spokes so that the lens created was a self-supporting structure.

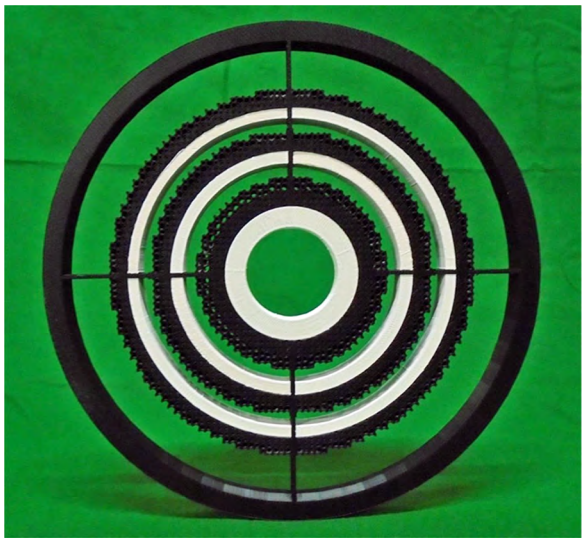

FIGURE 9. PREMIX and ABS 1X FDM lens (radius = 90mm).

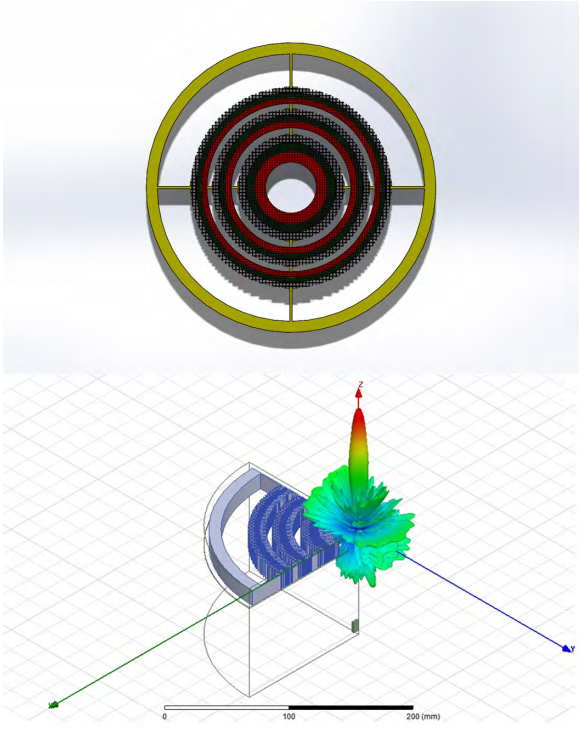

FIGURE 10. HFSS detailed model layout and pattern result.

In total, three lenses were fabricated including a SLA design, a hybrid-FDM design, and a 2X SLA design that was printed in quarters. Of note, PREMIX TP20280 filament was identified and imported from Norway. It is formulated to provide a high dielectric constant and a low loss tangent with the following quoted values at 1GHz ($\varepsilon_r = 4.4$, $\tan\delta = 0.004$). Note that Table 4 shows the values measured in this study which are for the bulk filament. This filament was easy to feed mechanically, even with a 0.4-mm nozzle. The required extrusion temperature was 260°C and the bed temperature was 110°C, which are both readily achievable.

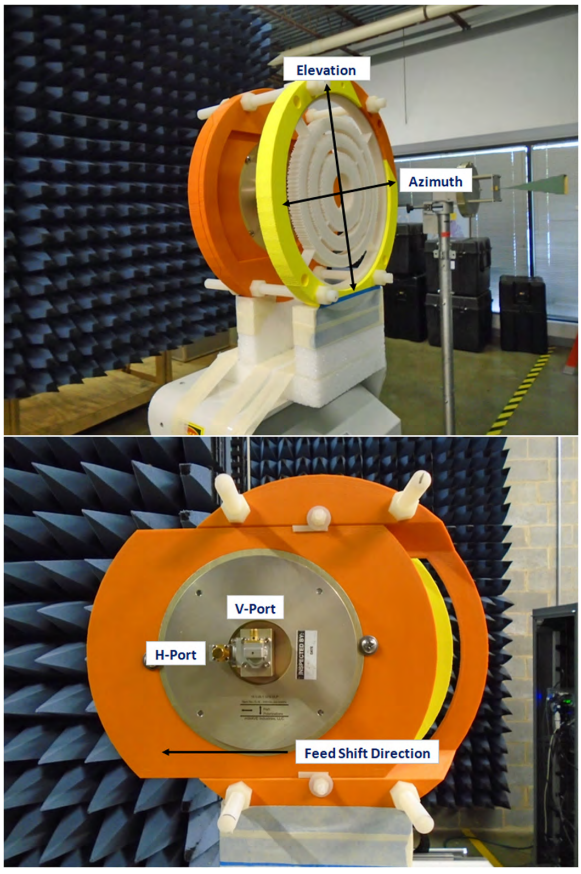

FIGURE 11. 3D printed lens and associated beam-steering test fixture hardware. 1X SLA lens (radius = 90mm).

V. MEASURED RESULTS

With the 3D printing material details defined, the HFSS modeling was re-visited (see Fig. 10) to verify the accuracy of the design. Modeling the individual dielectric hole structures significantly increased the computational mesh (and hence the memory space) required to run the models. This was compensated by using quartered symmetry planes to reduce the run times of the HFSS simulations. Ultimately, there was not an appreciable difference between the results from the bulk model and detailed models. So for future designs, verifying the layout using the simpler bulk model would be sufficient. When modeling the bulk material, it is important to account for the effects of the perforations in both the dielectric constant and loss tangent in HFSS – see equations (6) and (7).

Custom 3D printed test fixtures were fabricated to assist with measurement of the lens antennas. This included developing a means of custom tuning the feed location to assist with focusing of the lens, as well as offsetting the feed to facilitate a beam-steering study. Fig. 11 shows details of the mounting configurations on the near-field antenna range.

Swept gain and pattern measurements were performed utilizing an available near-field range. Prior to the measurements, the feed was focused and optimized for maximum gain. This occurred at 22GHz, which is slightly higher than the design frequency (of 20GHz). This was likely due to the

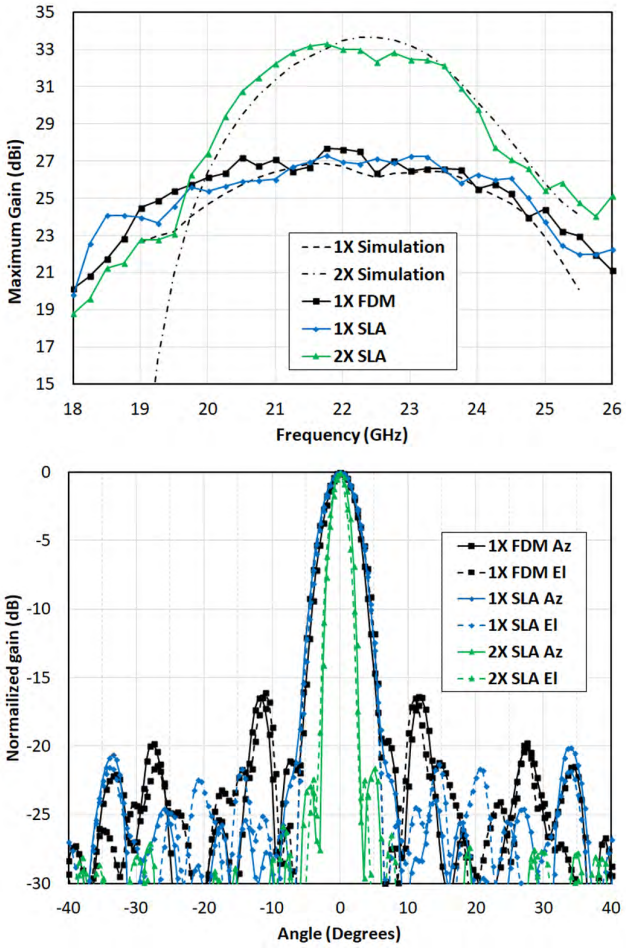

FIGURE 12. Measured swept gain (top) and 22GHz pattern results (bottom) for both SLA and FDM printed lenses.

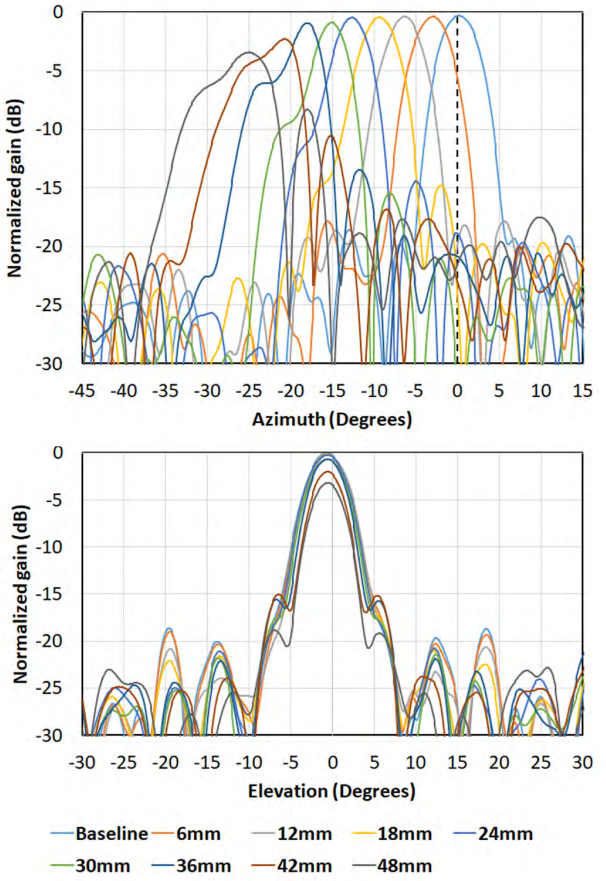

FIGURE 13. Measured results showing the beam-steering capability of the SLA printed lens at 22GHz.

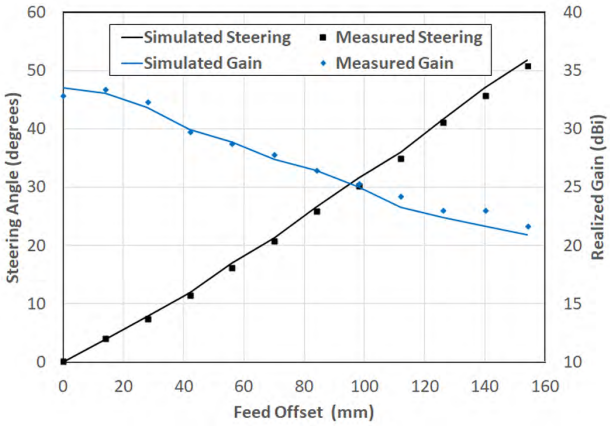

FIGURE 14. Comparison of measured and simulated beam-steering performance showing steering angle and gain for a linear feed offset.

performance of the feed used to illuminate the lens, which was a broadband dual-polarized 18-26.5GHz circular choke feed. Fig. 12 shows the gain and pattern performance of the SLA and FDM lenses. The gain of the SLA lens was 27.3-dBi, the FDM lens was 27.8-dBi, and the 2X SLA lens was 33.3-dBi, all measured at 22GHz. This corresponds to 30-35% efficiency, which correlates nicely with the simulated data.

In addition to the swept gain and pattern measurements, beam-steering performance was measured to evaluate the ability to point the lens off-axis without physically tilting the structure. Fig. 13 shows that $\pm 25^\circ$ is readily achievable with a maximum steering loss of 3-dB (at 25°). Steering was performed in one single plane as a proof of concept, but it would be trivial to implement this in both the azimuth and elevation planes. Of note, as the feed is translated to the edge of the lens, the sidelobes increase as one would expect due to over-illumination of the aperture edge boundary.

Measured and simulated beam-steering performance for the 2X lens is shown in Fig. 14. Agreement is very good, verifying that the bulk material model accurately accounts for changes in loss tangent due to air holes. Steering is accomplished by moving the feed off axis, so gain is reduced as lens illumination is decreased. Lens area also decreases geometrically with beam angle. As shown in Fig. 13, azimuthal beam width increases with steering angle, further reducing gain.

VI. CONCLUSIONS AND FUTURE DEVELOPMENT

The lenses designed for this study showed excellent agreement between simulation and measured data. The authors were able to successfully demonstrate multi-zone Fresnel

lenses constructed using SLA and FDM techniques. Overall gains in the range of 27-33dBi were achieved, in addition to beam-steering performance from ±25°. A core reason for the successful results was the measurement of the dielectric constant and loss tangent of every custom dielectric used in the lenses.

The next phase of exploration includes customizing the design to a specific problem scenario. Another area of development is to identify and characterize additional FDM materials that are higher epsilon and low loss, which would improve the overall efficiency of the structure. Since FDM filament has lower loss than SLA resin, and since we determined that high epsilon printing with larger air gaps improves efficiency, we will use these properties to improve our lenses. Another interesting technique is to incorporate high epsilon resins into the structure [22], which would allow more options in material choices.

The flexibility of 3D printing would allow for taking advantage of a continuous gradient in dielectric constant as a function of radius rather than discrete steps. The first 3D printed lenses mimic earlier construction techniques, including drilling of holes in bulk plastic, to create a desired dielectric constant. Each dielectric constant corresponds to one discretized choice of hole-size and spacing drilled into a particular bulk material. Rather than creating stair-stepped, uniform dielectric constants at various radii, a gradient could be created by continuously varying hole spacing or infill percentage as a function of radius. Since 3D printing can create arbitrary geometries; hole-size, shape, and spacing can be varied continuously. The authors envision an FDM print on a continuous spiral layout where the filament turns on/off. This geometry would provide the finest control of dielectric constant versus radius.

REFERENCES

[1] J. D. Krauss and R. J. Marhefka, "Lens Antennas," in *Antennas for All Applications*, 3rd ed. New York, NY, USA: McGraw-Hill, 2002, pp. 607–635.
[2] M. Imbert, A. Papió, F. De Flaviis, L. Jofre, and J. Romeu, "Design and performance evaluation of a dielectric flat lens antenna for millimeter-wave applications," *IEEE Antennas Wireless Propag. Lett.*, vol. 14, pp. 342–345, 2015.
[3] S. Zhang, R. K. Arya, S. Pandey, Y. Vardaxoglou, W. Whittow, and R. Mittra, "3D-printed planar graded index lenses," *IET Microw. Antennas Propag.*, vol. 10, no. 13, pp. 1411–1419, Nov. 2016.
[4] D. Isakov, C. J. Stevens, F. Castles, and P. S. Grant, "3D-printed high dielectric contrast gradient index flat lens for a directive antenna with reduced dimensions," *Adv. Mater. Technol.*, vol. 1, no. 6, 2016, Art. no. 1600072.
[5] H. D. Hristov and J. M. Rodriguez, "Design equation for multidielectric Fresnel zone plate lens," *IEEE Microw. Wireless Compon. Lett.*, vol. 22, no. 11, pp. 574–576, Nov. 2012.
[6] S. Zhang, "Design and fabrication of 3D-printed planar Fresnel zone plate lens," *Electron. Lett.*, vol. 52, no. 10, pp. 833–835, Apr. 2016.
[7] O. Wiener, "Zur theorie der refraktionskonstanten," *Berichteüber Verhandlungen Königlich-Sächsischen Gesellschaft Wisseschaften Leipzig Math.-Phys. Klasse*, Band 62, pp. 256–277, 1910.
[8] Formlabs. *What Does Resolution Mean in 3D Printing?* Accessed: Mar. 15, 2019. [Online]. Available: https://formlabs.com/blog/resolution-meaning-3d-printing/
[9] S. Bild. *Microns in 3D Printing: Do They Matter?* Additive Manufacturing in the Automotive Industry. Accessed: Mar. 15, 2019. [Online]. Available: https://blog.trimech.com/do-microns-matter-in-3d-printing
[10] Z. J. Larimore, M. S. Mirotznik, and P. E. Parsons, "Space filling curves for additive manufacturing of spatially graded dielectric structures," in *Proc. IEEE Int. Symp. Antennas Propag. (APSURSI)*, Jun./Jul. 2016, pp. 1937–1938.
[11] P. I. Deffenbaugh, R. C. Rumpf, and K. H. Church, "Broadband microwave frequency characterization of 3-D printed materials," *IEEE Trans. Compon., Packag., Manuf. Technol.*, vol. 3, no. 12, pp. 2147–2155, Dec. 2013.
[12] J. Baker-Jarvis, M. D. Janezic, and D. C. Degroot, "High-frequency dielectric measurements," *IEEE Instrum. Meas. Mag.*, vol. 13, no. 2, pp. 24–31, Apr. 2010.
[13] C. C. Courtney, "Time-domain measurement of the electromagnetic properties of materials," *IEEE Trans. Microw. Theory Techn.*, vol. 46, no. 5, pp. 517–522, May 1998.
[14] *Basics Of Measuring The Dielectric Properties of Materials*, Keysight Technol., Santa Rosa, CA, USA, Jan. 2019. [Online]. Available: http://literature.cdn.keysight.com/litweb/pdf/5989-2589EN.pdf
[15] M. N. Afsar, J. R. Birch, R. N. Clarke, and G. W. Chantry, "The measurement of the properties of materials," *Proc. IEEE*, vol. 74, no. 1, pp. 183–199, Jan. 1986.
[16] C. A. Balanis, "Circular cross-section waveguides and cavities," in *Advanced Engineering Electromagnetics*, Hoboken, NJ, USA: Wiley, 1989, pp. 470–535.
[17] R. S. Elliott, *Antenna Theory and Design*. Hoboken, NJ, USA: Wiley, 2003.
[18] F. Castles *et al.*, "Microwave dielectric characterisation of 3D-printed $BaTiO_3$/ABS polymer composites," *Sci. Rep.*, vol. 6, p. 22714, Mar. 2016. [Online]. Available: https://www.nature.com/articles/srep22714.
[19] Y. Wu, D. Isakov, and P. S. Grant, "Fabrication of composite filaments with high dielectric permittivity for fused deposition 3D printing," *Materials*, vol. 10, no. 10, p. 1218, 2017.
[20] K. T. Mathew, "Perturbation theory," in *Encyclopedia of RF And Microwave Engineering*. Hoboken, NJ, USA: Wiley, 2005.
[21] G. P. Lesage, *Dielectric Test Cavity for 3D Printing Filament*. Thingiverse. Accessed: Jul. 2, 2017. [Online]. Available: https://www.thingiverse.com/thing:2414931
[22] M. Yin, X. Y. Tian, L. L. Wu, and D. C. Li, "All-dielectric three-dimensional broadband Eaton lens with large refractive index range," *Appl. Phys. Lett.*, vol. 104, no. 9, 2014, Art. no. 094101.

JAMES M. MONKEVICH (M'97–SM'10) received the B.S. and M.S. degrees in electrical engineering specializing in antennas and electromagnetics from Virginia Tech., in 1993 and 1998, respectively.

He was with ManTech International Corporation, from 1993 to 1995, and Harris Corporation, from 1998 to 2001. Since 2001, he has been with the United States Government, Washington, DC, USA. He holds a patent and conducts a research related to novel antenna designs, additive manufacturing techniques, and RF systems integration.

GREGORY PETER LE SAGE (M'15) received the B.S., M.S., and Ph.D. degrees in electrical engineering from the University of California, Los Angeles, in 1991, 1994, and 1997, respectively, with a major in electromagnetics.

He was with the Lawrence Livermore National Laboratory, from 1997 to 2006. Since 2000, he has worked for the United States Government in Washington, DC, USA. He has authored or coauthored numerous journal articles and conference papers. He holds several patents. His research has included particle accelerators, high-power microwaves, lasers, miniature electronics, power sources, more recently 3D printing and scanning, CNC machining, and antenna design.